International Journal of Engineering & Technology, 7 (3.2) (2018) 575-579

International Journal of Engineering & Technology

Website: www.sciencepubco.com/index.php/IJET

Research paper

Reinforcement Corrosion Characteristics with Periodical Profile

Viktor Bondar[1], Liudmyla Bondar[2], Oleksandr Petrash[3]*

[1]Poltava National Technical Yuri Kondratyuk University, Ukraine
[2]Poltava National Technical Yuri Kondratyuk University, Ukraine
[3]Poltava National Technical Yuri Kondratyuk University, Ukraine
**Corresponding author E-mail: Alexandr_Petrash@ukr.net*

Abstract

The theoretical analysis of corrosion processes on the periodical profile reinforcement in low potential corrosion environment has been conducted using a mathematical model. The boundary between liquid and metal phases in the model was set by a sinusoidal laxly concaved profile. In this research, it's been suggested the hypothesis that mass transfer of cathodic and anodic depolarizers on the surface of corroborated reinforcement is defined by diffusion such that current density is constant on long distance from the boundary between the phases. The Laplacian equation has been solved by perturbation method representing concentrations as mathematical row by a small parameter. It has been analyzed the possibility of occurring a liquid coating under the concrete protective layer on the reinforcement surface in the contact spots between the ribs and reinforcement body. It's been discovered how the profile geometry impacts the distribution of corrosion current.

Keywords: *corrosion; current; reinforcement; profile; rib.*

1. Introduction

During the designing stage of reinforced concrete structures, some specific measures are applied in order to prevent a corrosion of reinforcement in them. There is a number of different methods of a reinforcement protection [1 – 4].
Nevertheless, external observations indicate that a failure of reinforced concrete structures caused by a reinforcement corrosion in them. At the initial stage, a model of reinforcement corrosion in concrete might be represented by a simple scheme: environment – concrete – reinforcement. But that model doesn't account for all the spectrum of existing interactions between its elements.
Thus, a shape of a structure, a reinforcement location in it, reinforcement profile shape cause an electrochemical heterogeneity on reinforcement surface.
In building reinforced concrete structures, the access front for depolarization (oxygen) to reinforcement might be one-sided (thick plates, beams, etc.), two-sided (thin plates), triple-sided (edges, thin-walled beams).
Concrete plays a significant role in reinforcement corrosion since it is in direct contact with a reinforcement in reinforced concrete structures. Different conditions of concrete have a significant impact on its corrosion features.
Concrete as a porous medium possesses sorption characteristics which leads to the accumulation of water and aggressive reagents in concrete layers. On the contrary, concrete porosity creates a gradient in depolarization coming from an external environment to the reinforcement.
A periodical profile can cause a concentration of changes in protection layer of concrete adjacent to reinforcement, thus, facilitate arising the intervals of different corrosion systems. Different concentration of depolarization (oxygen) at the top and bottom parts of reinforcement ribs with the periodical profile will cause a different density of corrosion current.
According to the laws of electrochemistry, the intervals of metals supplied by the less quantity of oxygen gain more negative potential and, under favorable conditions for galvanic pairs activity, are anodic.

2. Main Body

When reinforcement is in contact with the aggressive mixture, that accumulated inside of the protective layer of concrete, or exposed as a result of its damage, a set of common patterns remains under these conditions. The patterns specific to corrosion of steel immersed in a liquid electrolyte [5, 6].
The reinforcement roughness of periodical profile makes its surface not equally available in respect to diffusing component of electrolyte, which leads to significant deviations in the distribution of corrosion currents on reinforcement surface in the longitudinal direction [7 – 10].

2.1. Distribution of Electrode Areas on the Reinforcement with Periodical Profile in Conditions of Low Potential Energy

A theoretical analysis of corrosion processes in described conditions is conducted on the mathematical model in which a boundary between metal and liquid phases presented as sinusoidal laxly concaved profile (fig. 1).

$$y = H \cdot \sin kx , \quad (1)$$

where H – amplitude, L – period,
$k = 2\pi / L$, x, y – current coordinates, given that $Hk < 1$.

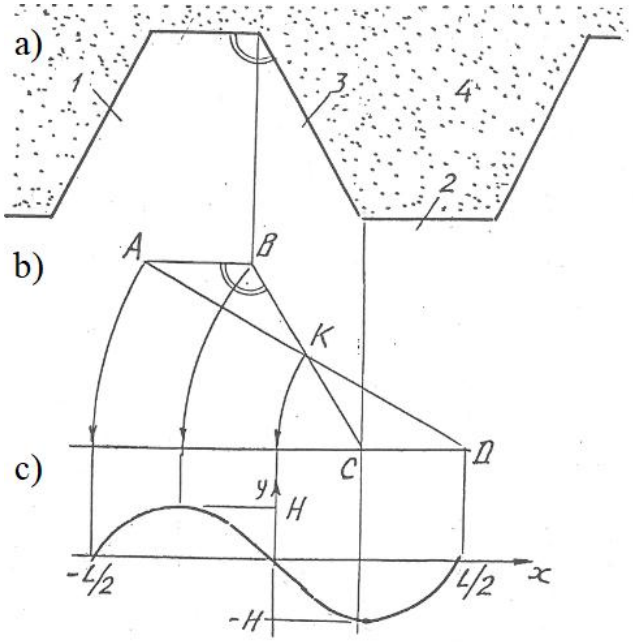

Fig. 1: The periodical profile reinforcement surface modeling: a – the longitudinal cross-section fragment of reinforcement; b – the reinforcement design fragment scheme; c – a model of the design fragment; 1 – the reinforcement rib; 2 – reinforcement rod; 3 – boundary phase; 4 – electrolyte

The sinusoidal profile is built based on a rough boundary (fig. 2) taken from a real geometry of periodical profile of reinforcement under the condition that $AB = BK = KC = CL$. The distance between points A and D is period L, and amplitude are defined by a distance of points B and C from AD line.

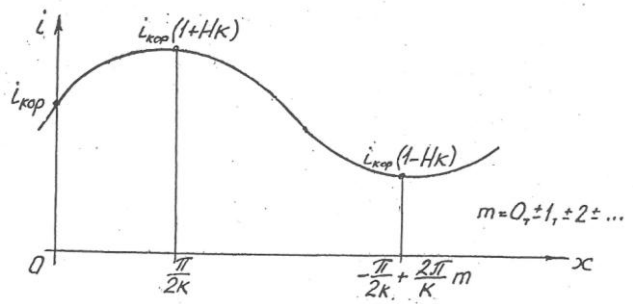

Fig. 2: The current distribution along the sinusoidal profile

Let us suggest that mass transfer of anodic and cathodic depolarizers at the surface of the reinforcement under corrosion is defined by a diffusion, the current density at long enough distances from phase boundaries is constant, and electrical current lines are parallel with each other and orthogonal to the surface of a reinforcement bar. Under these assumptions in stationary conditions the task comes down to a join solution of two-dimensional differential Laplace equations that describe diffusive field of anodic and cathodic depolarizers:

$$\Delta C = 0 , \quad (2)$$

under the following boundary conditions:
a condition of phases boundary shape is (1);
a condition of the current density continuity at long distances from boundary phases (regularity at ∞) is

$$-i = \sigma_1 \cdot \partial C^1 / \partial y = i_{cor} \text{ when } y \to +\infty , \quad (3)$$

$$-i = \sigma_2 \cdot \partial C^2 / \partial y = i_{cor} \text{ when } y \to -\infty . \quad (4)$$

the condition of processes conjunction on surface phases separation is given by

$$\sigma_1 \frac{\partial C^1}{\partial n} = \sigma_2 \frac{\partial C^2}{\partial n} ; \quad (5)$$

The condition of reinforcement surface equipotentiality (under a high conductivity of electrolytic environment and sinusoidal laxly concaved profile) potential of which equals the stationary potential is:

$$E_{sp} = f(C_{a0}; C_{C0}; i_a^0; i_c^0; E_a^0; E_c^0; i_{cor}) . \quad (6)$$

In the equations (3 – 6):
C^1 and C^2 – are the concentration of anodic and cathodic depolarizers; Z – a charge of diffusive ions; D – diffusion coefficient, F – Faraday's constant, i_{cor} –corrosion current density, dC/dn – derivative over normal to the profile, c_{a0} and c_{c0} – equally weighted concentrations of anodic and cathodic depolarizers, i_a^0 and i_c^0 – interchange currents, E_a^0 and E_c^0 – equally weighted potentials of anodic and cathodic depolarizers, and σ_1 and σ_2 are given by

$$\sigma_1 = z_a \cdot D_a \cdot F , \quad (7)$$

$$\sigma_1 = z_c \cdot D_c \cdot F , \quad (8)$$

Taking into account that $kH < 1$, equation (2) can be solved by disturbance method, representing the concentrations as sequences by minor parameter.
The following dimensionless variables have been introduced in Laplacian equation (2) and boundary conditions (3 – 5): $\bar{x} = kx$; $\bar{y} = ky$; $h = kH$; $\varphi = k\sigma \cdot C / i_{cp}$. Then

$$\frac{\partial^2 \vec{\varphi}}{\partial \vec{x}^2} + \frac{\partial^2 \vec{\varphi}}{\partial \vec{y}^2} = 0 \text{, that is } \Delta \vec{\varphi} = 0 \quad (9)$$

The boundary conditions (3, 4):

$$\frac{\partial \varphi^1}{\partial \bar{y}} = 1 \text{ when } \bar{y} \to +\infty \quad (10)$$

$$\frac{\partial \varphi^2}{\partial \bar{y}} = 1 \text{ when } \bar{y} \to -\infty \quad (11)$$

Condition (5) can be converted as follows:

$$\frac{\partial \varphi^1}{\partial \bar{y}} - h\cos\bar{x}\frac{\partial \varphi^1}{\partial \bar{x}} = \frac{\partial \varphi^2}{\partial \bar{y}} - h\cos\bar{x}\frac{\partial \varphi^1}{\partial \bar{x}} \text{ when } \bar{y} = h\sin\bar{x} \quad (12)$$

To simplify equations (2 – 12) the following variables were introduced:

$$w = \bar{x} ; \; v = \bar{y} - h\sin\bar{x} . \quad (13)$$

By substituting (13) into (7) the following equation has been obtained:

$$\frac{\partial^2 \vec{\varphi}}{\partial w^2} - 2h\cos\bar{x}\frac{\partial^2 \vec{\varphi}}{\partial w \partial v} + h^2\cos^2\bar{x}\frac{\partial^2 \vec{\varphi}}{\partial v^2} + h\sin W\frac{\partial \vec{\varphi}}{\partial v} + \frac{\partial^2 \vec{\varphi}}{\partial v^2} = 0 . \quad (14)$$

Substituting $w = \bar{x}$, (14) goes down to:

$$\left(1+h^2\cos^2 w\right)\frac{\partial^2\vec{\varphi}}{\partial v^2}+\frac{\partial^2\vec{\varphi}}{\partial w^2}-2h\cos W\frac{\partial^2\vec{\varphi}}{\partial w\partial v}+h\sin w\frac{\partial\vec{\varphi}}{\partial v}=0. \quad (15)$$

Boundary conditions (10 – 12) are transformed into:

$$\frac{\partial\varphi^1}{\partial v}=1 \text{ when } \bar{y}\to+\infty \quad (16)$$

$$\frac{\partial\varphi^2}{\partial v}=1 \text{ when } \bar{y}\to-\infty \quad (17)$$

$$\frac{\partial\varphi^1}{\partial v}+h^2\cos^2 w\frac{\partial\varphi^1}{\partial v}-h\cos w\frac{\partial\varphi^1}{\partial v}= \\ =\frac{\partial\varphi^2}{\partial v}+h^2\cos^2 w\frac{\partial\varphi^2}{\partial w}-h\cos w\frac{\partial\varphi^2}{\partial w}. \text{ when } v=0 \quad (18)$$

Neglecting the values containing the second and higher degrees of *h*, the following expression can be compiled:

$$\frac{\partial^2\vec{\varphi_0}}{\partial v^2}+\frac{\partial^2\vec{\varphi_0}}{\partial w^2}+h\left[\frac{\partial^2\vec{\varphi_1}}{\partial v^2}+\frac{\partial^2\vec{\varphi_1}}{\partial w^2}-2\cos w\frac{\partial^2\vec{\varphi_0}}{\partial w\partial v}+\sin w\frac{\partial\vec{\varphi_0}}{\partial v}\right]=0. \quad (19)$$

By fragmenting the latter equation over *h* the final form will be:

$$\frac{\partial^2\vec{\varphi_0}}{\partial v^2}+\frac{\partial^2\vec{\varphi_0}}{\partial w^2}=0; \quad (20)$$

$$\frac{\partial^2\vec{\varphi_1}}{\partial v^2}+\frac{\partial^2\vec{\varphi_1}}{\partial w^2}=2\cos w\frac{\partial^2\vec{\varphi_0}}{\partial w\partial v}-\sin\frac{\partial\vec{\varphi_0}}{\partial v}. \quad (21)$$

Similarly, boundary conditions (16 – 18) will become:

$$\frac{\partial\varphi_0^1}{\partial v}=1; \text{ when } v\to+\infty \quad (22)$$

$$\frac{\partial\varphi_0^2}{\partial v}=1; \text{ when } v\to-\infty \quad (23)$$

$$\frac{\partial\varphi_0^1}{\partial v}=\frac{\partial\varphi_0^2}{\partial v}; \text{ when } v=0 \quad (24)$$

$$\frac{\partial\varphi_1^1}{\partial v}=0; \text{ when } v\to+\infty \quad (25)$$

$$\frac{\partial\varphi_1^2}{\partial v}=0; \text{ when } v\to-\infty \quad (26)$$

$$\frac{\partial\varphi_1^1}{\partial v}-\cos w\frac{\partial\varphi_0^1}{\partial w}=\frac{\partial\varphi_1^2}{\partial v}-\cos w\frac{\partial\varphi_0^2}{\partial w} \text{ when } v=0 \quad (27)$$

After simplifying equations (1 – 8) and boundary condition (27) the system of equations goes down to:

$$\frac{\partial^2\vec{\varphi_1}}{\partial w^2}+\frac{\partial^2\vec{\varphi_1}}{\partial v^2}=-\sin w; \quad (28)$$

$$\frac{\partial^2\varphi_1^1}{\partial v}=0; \text{ when } v\to+\infty \quad (29)$$

$$\frac{\partial^2\varphi_1^2}{\partial v}=0; \text{ when } v\to-\infty \quad (30)$$

$$\frac{\partial\varphi_1^1}{\partial v}=\frac{\partial\varphi_1^2}{\partial v}. \text{ when } v=0 \quad (31)$$

Equation (28) is inhomogeneous differential Laplacian equation (Poisson's equation), but since $\varphi_1=\sin w$ is its partial solution, than, by substituting $\varphi_1=F+\sin w$, it's possible to convert it into homogeneous Laplacian equation for the following function:

$$\frac{\partial^2\vec{F}}{\partial V^2}+\frac{\partial^2\vec{F}}{\partial W^2}=0. \quad (32)$$

The solution of (32) can be found by Euler-Fourier method in the following form:

$$F(v,w)=V(v)\cdot W(w), \quad (33)$$

where $V(v)$, $W(w)$ – are the new unknown functions.

The final solution for Laplacian equations is as follows:

$$\varphi^1=V+h\left[-e^{-V}\left(A\sin W+B\cos W\right)+\sin W\right] \\ \varphi^2=V+h\left[-e^{-V}\left(A\sin W+B\cos W\right)+\sin W\right] \quad (34)$$

Considering the function *C* and variables *x*, *v* and using formulas $w=\bar{x}$; $\bar{x}=kx$; $\bar{y}=ky$; $\varphi=k\sigma\cdot C/i_{cp}$, the following solution to equations (2 – 6) has been obtained:

$$C^1\equiv C_a=\frac{i_{cor}}{k\cdot\sigma_a}\left[V-h\left(-e^{-V}\left(A\sin kx+B\cos kx\right)+\sin kx\right)\right] \quad (35)$$

$$C^1\equiv Cc=\frac{i_{cor}}{k\cdot\sigma_k}\left[V+h\left(-e^{-V}\left(A\sin kx+B\cos kx\right)+\sin kx\right)\right], \quad (36)$$

Where $V=ky-h\sin kx$, $h=kH$, A and B – integration constants. The distribution of the anodic corrosion current over the sinusoidal profile at initial stage is

$$i_a(x)=i_{cor}\left[1+h\cdot\left(A\cdot\sin kx+B\cdot\cos kx\right)\right] \quad (37)$$

For the determination of *A* and *B* constants equation (37) is used. When cathodic and anodic reaction is defined by diffusion, the distribution of corrosion current can be defined by

$$i_a(x)=i_{cor}\left(1+Hk\sin kx\right). \quad (38)$$

Equation (38) coincides with Wagner's equation for the processes of metal polishing and deposition under the condition of constant potential profile or constant concentration of dissolving and depositing metal.

Using the analogic calculations, it is possible to obtain equations of corrosion current distribution for the other kinetic conditions of the inherent reactions course.

Thus, the obtained results allow assessing the corrosion processes in a wide range of initial data. From equation (38) it's getting clear that the maximum density of the current will take place when *sinkx = 1*, and minimum – when *sinkx = -1*.

That results in smoothing process of a reinforcing bar. As a corrosion velocity increases (i_{cor}), the unevenness in current distribution increases.

The geometry of reinforcement profile has a significant impact on corrosion current distribution.

Using Faraday's law, it's possible to describe the change of profile amplitude in time:

$$-dH=\frac{M}{\rho\cdot z_a\cdot F}\cdot\left(i_v-i_{vp}\right)\cdot dt, \quad (39)$$

where *M* and ρ – molecular mass and density of dissolving metal,

i_v, i_{vp} – the current density of dissolving metal at the top and bottom of a rib,
z_a – valence of anodic depolarizer ions,
F – Faraday's constant.
Since i_v-iv_p=$[(1+Hk)+(1-Hk)]$ ·i_k=$2i_k$·kH, then (39) can be modified to the following form:

$$dH/H=-Adt, \quad (40)$$

where $A = (M/(\rho \cdot z_a \cdot F)) \cdot 2i_{cor} \cdot K$.
The common solution for equation (40) is $lnH = -At+C$. Substituting the initial conditions $H|_{t=0}=H_0$, the solution of (40) will be obtained in the following form:
$lnH = -At + lnH_0$, which goes down to

$$H = H_0 \cdot e^{-At} \quad (41)$$

Assuming that the thickness of the corroborated metal is $\delta=2M \cdot t/(\rho \cdot z_a \cdot F)$, than (41) becomes

$$H = H_0 \cdot e^{-\delta K}. \quad (42)$$

Thus, analyzing the (42) it's obviously that the best corrosion characteristics (assuming that the thickness of corroborated metal is even) have the profiles with the least value of "K".

2.2. Surface Wetting of the Periodical Profile Reinforcement

During the research of corrosion processes on the reinforcement surface, it is necessary to account for physical and chemical phenomena that occurs when liquid is in contact with a solid surface. First of all, there is a process of liquid spreading until the edge angle is formed. Its boundaries are defined by the vector direction of surface tension between the "liquid-gas" and "metal-liquid" environments (σ_{lg} and σ_{ml}).
Surface wetting of periodical profile reinforcement has a set of features compared to flat surface reinforcement. The ribs on the reinforcement surface lead to a respective increasing in specific free energy surface (surface tension):

$$\sigma_{ml}^{S} = K \sigma_{ml}, \quad (43)$$

where σ_{ml}^{S} – is a surface tension of liquid on periodical profile reinforcement;
σ_{ml} – is a surface tension on flat surface reinforcement;
K – is the increasing of liquid contact area on a surface of periodical profile compared to the flat surface reinforcement.
According to Ventsel-Deriagyn equation:

$$cos\theta^{P} = K \cdot \theta, \quad (44)$$

where θ^{P}, and θ are the edge angles of liquid wetting on a surface of periodical and flat profile reinforcement.
Since $K > 1$, $cos\theta^{P} > cos\theta$, and $\theta^{P} < \theta$, that is periodical profile of reinforcement leads to decreasing of the edge angle, and improvement in reinforcement wetting.
The edge angle formed on a surface of periodical profile reinforcement θ^{P} (fig. 4) is defined by the edge angle θ and angle φ that characterizes tilts of orthogonal ribs.

$$\theta^{P} = \theta+\varphi. \quad (45)$$

Angle φ can be determined by the formula:

$$tg\ \varphi = - dy/dx. \quad (46)$$

Angle φ is variable and depends on the contact place between a liquid boundary and reinforcement surface. According to (46), it defines the value of the edge angle hysteresis.

On the idealized surface of the periodical profile reinforcement (fig. 5) the rib height can be estimated by

$$y = h \cdot (1 + cos\ 2\pi \cdot x/t), \quad (47)$$

where y, h – are the instant and maximum heights of a rib respectively;
t – is the distance between the neighboring ribs.
Fron equations (46) and (47) it's possible to conclude that the expression for φ will be:

$$\varphi = tg^{-1}[(2\pi \cdot h/t) \cdot sin(2\pi \cdot x/t)]. \quad (48)$$

The actual value of φ change varies between minimum and maximum, that is $\varphi_{min} \le \varphi \le \varphi_{max}$. The maximum φ_{max} will be obtained when $sin\ (2\pi \cdot x/t) = 1$, and minimum – when $(2\pi \cdot x/t) = -1$.

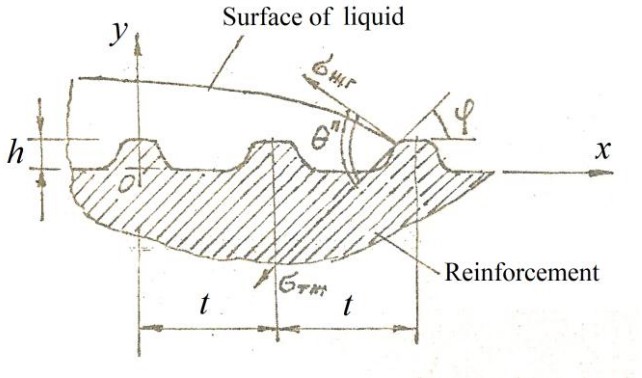

Fig. 5: The idealized surface of the periodical profile reinforcement

Table 1 and fig (6). show the values of φ_{max} and K of convenient periodical profile reinforcement from #5 to #50 for different h/t ratios.

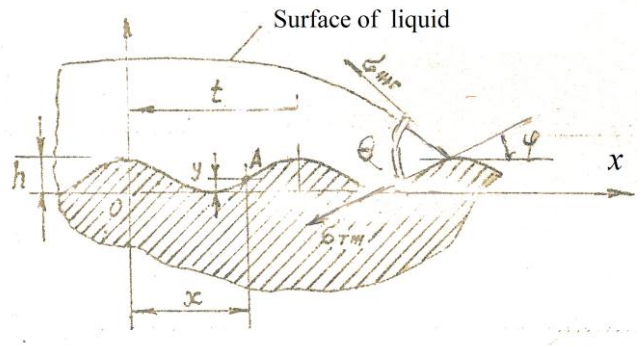

Fig. 6: The idealized surface of the periodical profile reinforcement with the sinusoidal profile

Table 1. φ_{max} and K values for periodical profile reinforcement

#	h/t	K	φ_{max}	#	h/t	K	φ_{max}
6	0.1	1.38	32.13	22	0.187	1.5	48.19
8	0.15	1.39	43.29	25	0.187	1.48	48.19
10	0.143	1.53	41.92	28	0.222	1.59	54.31
12	0.178	1.61	48.19	32	0.2	1.53	51.47
14	0.178	1.56	48.19	36	0.208	1.57	52.56
16	0.187	1.59	48.19	40	0.208	1.55	52.56
18	0.187	1.55	48.19	45	0.2	1.55	51.47
				50	0.2	1.53	51.47

3. Conclusion

The developed mathematical model allows estimating the corrosion processes on the periodical profile reinforcement in a wide range of initial data.
The theoretical analysis of the model reveals that distribution of corrosion current is significantly influenced by the geometry of a reinforcing bar profile.

The smoothening effect will be increased by a higher number of the periodical profile ribs.

When the corrosion velocity increases, the inhomogeneity of the corrosion current distribution over the periodical profile reinforcement surface increases too.

Adequacy of the developed model is confirmed by the experimental research of the rod reinforcement segments.

References

[1] S. Yogesha, and A. Chitharanjan Hegde, "Corrosion Resistant Zn-Co Alloy Coatings Deposited Using Saw-tooth Current Pulse", *Bulletin of Materials Science*, Vol.34, No.7, (2011), pp.1699-706, Accessed May 9, 2018. doi:10.1007/s12034-011-0380-1.

[2] Sun, Desheng, Peter Monaghan, William A. Brantley, and William M. Johnston, "Potentiodynamic Polarization Study of the in Vitro Corrosion Behavior of 3 High-palladium Alloys and a Gold-palladium Alloy in 5 Media", *The Journal of Prosthetic Dentistry*, Vol.87, No.1, (2002), pp:86-93, Accessed May 9, 2018. doi:10.1067/mpr.2002.121239.

[3] Soler, Ya. I., and D. Yu. Kazimirov, "Bearing Surface Area of Plate Macrorelief and Ways of Increasing It in the Course of Grinding Parts Made of Corrosion-Resistant Steel by Means of Aerobor Grinding Wheels", *Chemical and Petroleum Engineering*, Vol.52, No.3-4, (2016), pp.217-23, Accessed May 9, 2018. doi:10.1007/s10556-016-0178-5.

[4] Feliciano, Flávio Felix, Fabiana Rodrigues Leta, and Fernando Benedicto Mainier, "Texture Digital Analysis for Corrosion Monitoring", *Corrosion Science*, Vol.93, (2015), pp.138-47, doi:10.1016/j.corsci.2015.01.017.

[5] Lazzari, Luciano, "Statistical Analysis of Corrosion Data", *Engineering Tools for Corrosion*, (2017), pp.131-48, doi:10.1016/b978-0-08-102424-9.00008-2.

[6] Singh, D. D., N., and T. Venugopalan, "Understanding the Corrosion and Remedial Measures to Control the Deterioration of Reinforcement Steel Bars by Modification in Their Chemistry and Application of Surface Coatings", *Transactions of the Indian Institute of Metals*, Vol.66, No.5-6, (2013), pp.677-87, doi:10.1007/s12666-013-0335-x.

[7] Nürnberger, U., "Corrosion of Metals in Contact with Mineral Building Materials", *Corrosion of Reinforcement in Concrete*, 2007, pp.1-9, doi:10.1533/9781845692285.1.

[8] Hariri, Mohiedin Bagheri, Sajad Gholami Shiri, Yadollah Yaghoubinezhad, and Masoud Mohammadi Rahvard, "The Optimum Combination of Tool Rotation Rate and Traveling Speed for Obtaining the Preferable Corrosion Behavior and Mechanical Properties of Friction Stir Welded AA5052 Aluminum Alloy", *Materials and Design*, Vol.50, (2013), pp.620-34, doi:10.1016/j.matdes.2013.03.027.

[9] Zhang, Jieying, and Zoubir Lounis, "Sensitivity Analysis of Simplified Diffusion-based Corrosion Initiation Model of Concrete Structures Exposed to Chlorides", *Cement and Concrete Research*, Vol.36, No.7, (2006), pp.1312-1323, doi:10.1016/j.cemconres.2006.01.015.

[10] Popova, A.V., Kremenetsky, V.G., Solov'ev, V.V., Chernenko, L.A., Kremenetskaya, O.V., Fofanov, A.D., Kuznetsov, S.A., "Standard rate constants of charge transfer for Nb(V)/Nb(IV) redox couple in chloride-fluoride melts: Experimental and calculation methods", *Russian Journal of Electrochemistry*, Vol.46, No.6, (2010), pp.671-679, doi: 10.1134/S1023193510060121